

Gain variations as induced by the diffuse night sky background: the ASTRI-Horn experience



ASTRI Project collaboration

D. Impiombato,^{a,1} A.A. Compagnino,^{b,2} T. Mineo,^b O. Catalano,^b S. Giarrusso,^b M.C. Maccarone,^b

^aINAF, Osservatorio Astronomico di Padova, Vicolo Osservatorio 5, 35122, Padova, Italy

^bINAF, Istituto di Astrofisica Spaziale e Fisica Cosmica di Palermo, via U. La Malfa 153, I-90146 Palermo, Italy

E-mail: Domenico.Impiombato@inaf.it

ABSTRACT: ASTRI-Horn is the prototype of the nine telescopes that form the ASTRI Mini-Array, under construction at the Teide Observatory in Spain, devoted to observe the sky above 10 TeV. It adopts an innovative optical design based on a dual-mirror Schwarzschild-Couder configuration, and the camera, composed by a matrix of monolithic multipixel silicon photomultipliers (SiPMs) is managed by ad-hoc tailored front-end electronics based on a peak-detector operation mode. During the Crab Nebula campaign in 2018-2019, ASTRI-Horn was affected by gain variations induced by high levels of night sky background. This paper reports the work performed to detect and quantify the effects of these gain variations in shower images. The analysis requested the use of simultaneous observations of the night sky background flux in the wavelength band 300-650 nm performed with the auxiliary instrument UVscope, a calibrated multi-anode photomultiplier working in single counting mode. As results, a maximum gain reduction of 15% was obtained, in agreement with the value previously computed from the variance of the background level in each image. This ASTRI-Horn gain reduction was caused by current limitation of the voltage supply. The analysis presented in this paper provides a method to evaluate possible variations in the nominal response of SiPMs when scientific observations are performed in the presence of high night sky background as in dark or gray conditions.

KEYWORDS: ASTRI-Horn; Imaging Atmospheric Cherenkov Telescopes; SiPM

¹Corresponding author.

Contents

1	Introduction	1
2	The ASTRI-Horn	2
3	Data reduction and analysis	5
3.1	Analysis of the p.e. distributions	7
4	Results and Discussion	10
5	Summary and Conclusions	12

1 Introduction

The very-high-energy (VHE) γ -ray astronomy plays a crucial role in the exploration of the most violent non-thermal phenomena in the Universe. The scientific target extends from the origin of cosmic rays and dark matter to the γ -rays production in a large variety of galactic and extra-galactic sources. The feasibility of such studies is based on the availability of effective ground-based techniques for the detection of γ -radiation in a very broad energy region ranging from a few tens of GeV to hundreds of TeV. The turning point for these observations came from the Imaging Atmospheric Cherenkov Telescopes (IACTs) that observe the Cherenkov light in the air shower generated by the interaction of γ photons with the Earth's atmosphere. The IACT technique was pioneered by the Whipple collaboration and led to the discovery of TeV emission from the Crab Nebula in 1989 [1]. After that, small arrays of IACTs, firstly HEGRA [2] and then VERITAS[3], started the era of stereoscopic observations for the study of VHE γ -ray astronomical sources. The installation of further complex IACT instruments as MAGIC [4] and H.E.S.S. [5] allowed us for a strong increase of the number of discovered sources in a few years period.

The success achieved by these instruments (all of them with a single mirror optics and cameras equipped with photomultiplier tubes) has driven the international VHE astronomy community towards the design of new-generation IACT telescopes, with the intent to enlarge the observable energy region as well as to reach a wider field of view. Double mirror optics and cameras with different sensors, equipped with a properly fast electronics, are the main objectives of such new designs.

In the field of new camera sensors, the Silicon Photo-Multipliers (SiPMs) represent the ideal choice offering all the advantages of a solid state device such as robustness, low operative voltage, high time resolution, insensitivity to magnetic fields. Moreover, in recent decades, the nuclear physics, medical physics and astrophysics communities have given more impact to the partnership with its suppliers obtaining good improvements in the SiPMs performance. Several drawbacks have been considerably reduced, so obtaining the lowering of the breakdown voltage and of the

optical cross-talk occurrences, a higher photon-detection-efficiency and a reduction almost twofold of the gain dependence on temperature variations. It is precisely this latter feature that represents a major improvement to avoid significant variations in the pixels gain of the sensor. In addition, the performance of today's SiPMs makes it possible to observe in presence of a very high level of night sky background (NSB) without any damage and loss of dynamic range induced by high level of current absorption.

Thanks to the previously described improvements, several new-generation IACT telescopes, first of all the small instrument FACT [6], have chosen SiPMs for their cameras. Among them, the ASTRI-Horn telescope whose experience concerning gain variations induced by the diffuse NSB is described in the present paper.

ASTRI-Horn [7] is a 4-m class IACT telescope developed by the Italian National Institute for Astrophysics (INAF) in the context of the Cherenkov Telescope Array (CTA) [8]. The telescope structure and its optics system have been chosen for the small-sized telescopes to be installed at the CTA southern site. At the same time, the complete ASTRI-Horn is the prototype of the nine telescopes that form the ASTRI Mini-Array [9] under construction at the Teide Observatory, Canary Islands, Spain, that will be able to study bright sources ($\sim 10^{-12}$ erg cm^{-2} s^{-1} at 10 TeV) with an angular resolution of $\sim 3'$ and an energy resolution of $\sim 10\%$ at an energy of about 10 TeV [10].

The ASTRI-Horn telescope is characterized by an optical system based on a dual-mirror Schwarzschild-Couder design and a camera at the focal plane composed of multipixel SiPM sensors managed by a fast read-out electronics specifically designed. ASTRI-Horn is located on Mt. Etna, Serra La Nave, Italy, at the INAF 'M.C. Fracastoro' observing station [11]. Among the various auxiliary instrumentation present on site, mainly devoted to the telescope pointing and local atmosphere monitoring, ASTRI-Horn is equipped with UVscope [12], a multi-anode photomultiplier instrument working in single photon counting to measure the diffuse NSB in the wavelength band 300-650 nm band.

Using data acquired in December 2018, during the commissioning phase of the telescope, it was possible to correlate the level of diffuse NSB measured by UVscope with the signal detected by the ASTRI-Horn camera [13]. Authors found that when the NSB level detected by UVscope was lower than ~ 4700 $\text{ph m}^{-2} \text{ns}^{-1} \text{sr}^{-1}$ (1.43 $\text{ph m}^{-2} \text{ns}^{-1} \text{deg}^{-2}$) the ASTRI-Horn camera response was nominal, while above this level it was affected by a limit in the power supply that reduced the operative voltage of all its SiPM sensors. The aim of this paper is to demonstrate that the effects of this limitation are also present in the signals produced by the detected showers. After some technical information on ASTRI-Horn telescope and UVscope (Sect. 2), the data reduction and analysis are presented in Sect. 3. Results and discussion are presented in Sect. 4; conclusions follow in (Sect. 5).

2 The ASTRI-Horn

The ASTRI-Horn telescope is an end-to-end prototype of the 4-m class IACTs. Its name has been chosen in honour of the Italian astronomer Guido Horn D'Arturo who pioneered the use of segmented primary mirrors in astronomy [14]. ASTRI-Horn (see Fig.1) is the first Cherenkov telescope to adopt a dual-mirror optical configuration and among the first to use SiPM sensors that, in ASTRI-Horn, are read-out by a very fast and specifically designed electronics. A complete

description of the telescope can be found in several papers and references therein (see e.g. [15]). Here we summarize some general info together with those features that are of main interest for the analysis presented in this paper.



Figure 1. ASTRI-Horn, the dual-mirror Cherenkov telescope installed on Mt.Etna, Italy, at the INAF 'M.C. Fracastoro' observing station (1740 m a.s.l.). On the right panel it is visible the small UVscope instrument mounted under the primary mirror structure of the ASTRI-Horn telescope.

The telescope optical system is based on a modified dual-mirror Schwarzschild-Couder configuration, [16] with the camera located between the secondary and primary mirror. This camera is composed of 8×8 multipixel SiPM sensors chosen for providing a compact system [17] and organized in 21 Photon Detection Modules (PDM) reaching a full field-of-view (FoV) of 7.6° [17]. The camera is thermally controlled to keep the temperature varying in a small interval ($\pm 2^\circ\text{C}$) around the nominal value of 15°C in order to control the gain stability.

Differently from other Cherenkov telescopes that use the standard sampling technique, the ASTRI-Horn camera front-end electronics is based on a custom peak-detector operation mode to capture and hold the maximum value of the analog signal from the SiPM pulses [17, 18]. This is accomplished thanks to the application-specific integrated circuit (ASIC) CITIROC (Cherenkov Imaging Telescope Integrated Read Out Chip) [19] properly customized for ASTRI-Horn. The read-out electronics is AC-coupled to the detector output blocking any slow varying signal as the NSB or star light in the FoV. However, Poisson fluctuations of these signals are detected by the electronics as fluctuations around the zero level (pedestal). The standard deviation of these fluctuations is mainly proportional to the NSB flux, being both the intrinsic electronic noise and the SiPM dark current much lower [20].

The ASTRI-Horn camera is also equipped with a fiber optics system (FOC) whose light, continuously or pulsed, illuminates the detector allowing for a further increase in the gain uniformity over the focal plane with off-line analysis.

A voltage distribution board (VDB) constituted by a main board and 21 daughter boards provides the required regulated power to all the electronics devices of the camera up to a limit current of ~ 6 mA [18].

Eventually, two light-tight lids prevent accidental sunlight exposure of the focal surface detectors [17].

ASTRI-Horn implements a topological trigger in order to reduce background induced events. In particular the trigger is activated when a given number of contiguous pixels within a PDM measures a signal above a given threshold. Both the number of contiguous pixels required for the trigger and the signal threshold are set by user to minimize the number of false triggers.

ASTRI-Horn is equipped with UVscope, a light detector mainly devoted to measure the diffuse NSB in the wavelength band 300–650 nm [12]. Mounted under the primary mirror structure of the telescope and co-aligned with the ASTRI-Horn camera axis, UVscope takes data contemporarily to and independently from the ASTRI-Horn camera acquisitions. Its light sensor is a calibrated multi-anode photomultiplier tube (MAPMT) with 8×8 pixels working in single photon counting mode [21] to keep the electronic noise negligible. The angular aperture of each UVscope pixel (0.55′) is equivalent to about 3×3 pixels of the ASTRI-Horn camera, that makes its FoV coincident with the one relative to the 3×3 central PDMs of the ASTRI-Horn camera (identified in red colour in Fig. 2).

The ASTRI-Horn scientific capability was proven by the detection of the Crab Nebula emission above an energy threshold of ~3 TeV with a statistical significance of 5.4 σ . The relative observations were carried out in December 2018 during the telescope commissioning phase for a total on-source observing time of 12.4 h, and an equal duration of the off-source exposure [7]. The same data also demonstrated the utility of UVscope in checking and quantifying the discrepancies with respect to the nominal working of the camera [13].

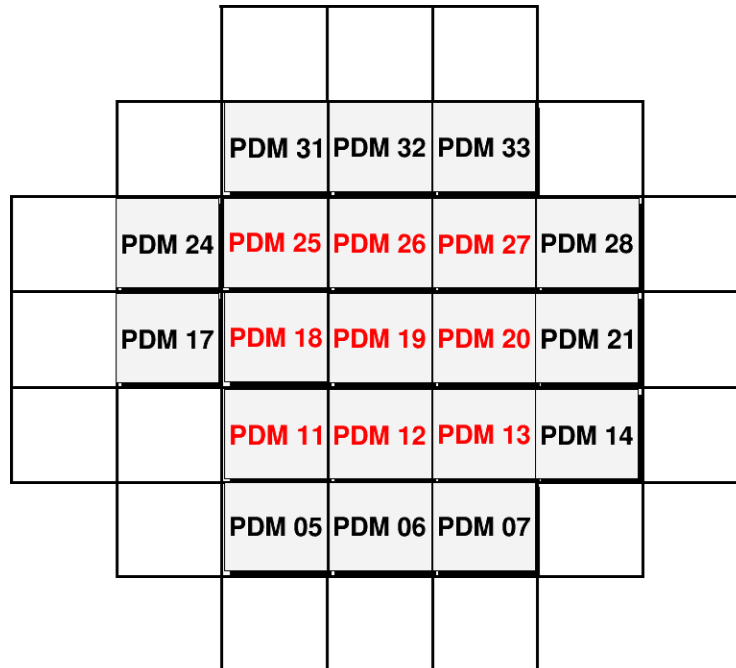


Figure 2. Geometric arrangement of PDM on ASTRI-Horn focal plane. The nine central PDMs used in this work are highlighted in red; they roughly cover the FoV seen by UVscope.

3 Data reduction and analysis

Main task of our analysis is to check and quantify gain variations induced by high levels of the NSB in the detected signals. To this purpose, we investigated how the photoelectrons (p.e.) distribution of the detected showers varies in presence of high NSB fluxes. In particular, whenever relatively small gain variations are present in the ASTRI-Horn camera, a given particle/photon energy would produce a lower signal without changing the shape of the p.e. distribution whose mathematical model, as directly derived from data, is a power law. In fact, let us define p_0 and p_1 the normalization and the index of the power law of the distribution; $N_r(p.e.)$ that is the number of pixels with p.e. signal relatively to the nominal reference gain G_r , is given by :

$$N_r(p.e.) = p_0(G_r) p.e.^{p_1} \quad (3.1)$$

considering that $p_0(G_n)$ is the scale factor of the distribution relative to the new gain G_n , the expected distribution becomes:

$$N_n(p.e.) = p_0(G_r) \left(\frac{G_n}{G_r} p.e.\right)^{p_1} = p_0(G_n) p.e.^{p_1} \quad (3.2)$$

From the formula, it is evident that a proportional variation of the normalization parameter follows any gain variation.

For our analysis, we selected ASTRI-Horn and UVscope contemporary acquisitions in six time intervals relative to different NSB levels during the 2018 December 7–8 observation night [12, 13]. Table 1 lists the selected Run IDs and the sequence numbers of the ASTRI-Horn considered files, together with the starting times, exposures, and pointing directions (the UVscope data, acquired along all the night towards the same ASTRI-Horn pointings, are stored in a unique single file). The plot of the temporal evolution of the NSB flux measured by UVscope every second along all night is shown in the top panel of Fig. 3. The bottom panel of the figure shows, for comparison, the root mean squared (*RMS*) of background fluctuations measured in the central PDMs of ASTRI-Horn camera, and averaged in ~ 2 minutes [13]. This *RMS* was obtained as σ of the p.e. distribution around the pedestal after subtracting showers and star signals.

The three pointings Run ID 1453(006), 1456(002) and 1456(003), indicated with red dashed vertical lines in Fig. 3, were not affected by current limitation, at difference with the observations identified within the blue lines (Run ID 1454(000), 1455(000) and 1455(005)). The difference in the ASTRI-Horn response can be easily inferred by comparing the almost absence of variations in the *RMS* between the first run (ID 1453(006); $T = 0.7$ h) and the second one (ID 1454(000); $T = 1.4$ h) with respect to UVscope data whose intensity increases by $\sim 25\%$.

Only the nine central PDMs (see Fig. 2) were considered in the analysis allowing for a comparison with the results presented in our previous paper [13]. Data were relative to the LG chain, being the HG not available at the considered observing time. The first step of the data reduction concerns the calibration of the pixels gain. This was performed with the method explained in [13] and with the data listed in Table 2 and 3 of the same paper.

In our analysis, we are interested in pixels whose signal is produced by showers and whose content is well above the NSB. We then considered only triggered events with at least one pixel with more than 50 p.e., value empirically determined. From these events, the p.e. distributions relative to

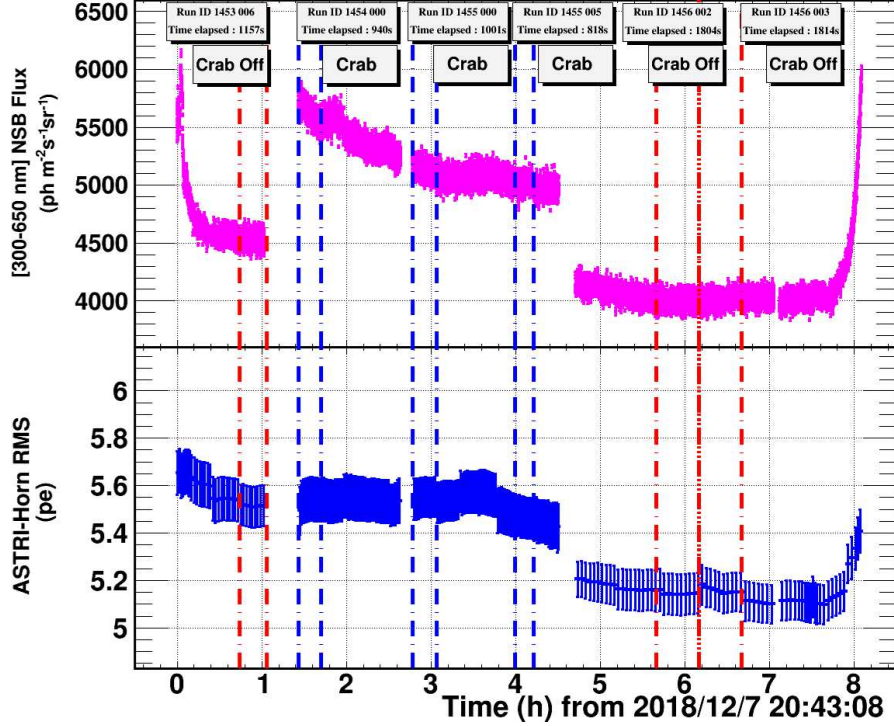


Figure 3. Temporal evolution of the NSB flux measured by UVscope (top panels) relative to the observing night 2018 December 7-8; the bottom panel shows the contemporary evolution of the RMSs measured by ASTRI-Horn. The vertical dashed lines limit the considered time intervals; the red colour is relative to intervals not affected by current limitation, while blue lines show the periods when the camera presents nominal behaviour; the red vertical dashed-dotted line indicates the time separation between two runs.

Table 1. Observation log of ASTRI-Horn data used in this paper.

Run ID (Seq.)	UTC Starting Date (d h:m:s)	Exposure (s)	Pointing RA,Dec
1453 (006)	2018/12/07 21:27:10	1157	46.13°, 22.01° (Crab Off)
1454 (000)	2018/12/07 22:09:16	940	83.63°, 22.01° (Crab)
1455 (000)	2018/12/07 23:30:08	1001	83.63°, 22.01° (Crab)
1455 (005)	2018/12/08 00:42:25	818	83.63°, 22.01° (Crab)
1456 (002)	2018/12/08 02:23:00	1804	121.13°, 22.01° (Crab Off)
1456 (003)	2018/12/08 02:53:04	1814	121.13°, 22.01° (Crab Off)

$N1 \geq 5$ contiguous pixels with more than $S1 \geq 13$ p.e. per pixel, were accumulated. This procedure produces cleaned images adequate for our analysis. In accumulating the p.e. distributions, we excluded pixels with bright stars, as in [13]. Including these pixels gives compatible results but with lower statistical significance. Fig.4 shows the average p.e. number of all the detected signals (bright stars included) relative to Run 1453(006). From the plot, it is well evident the capability of ASTRI-Horn camera to detect stars, as already presented in [13].

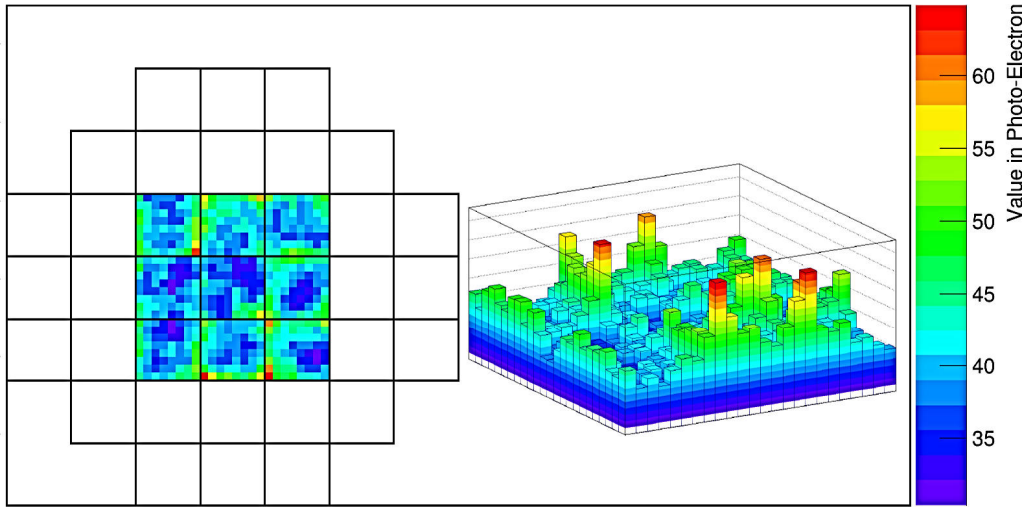


Figure 4. Average p.e. of the cleaned image detected in central PDMs of the run 1453(006). Pixels with higher values (coloured in red) include contribution from bright stars in the field of view.

3.1 Analysis of the p.e. distributions

The p.e. distributions from the central PDMs were accumulated for each run; as an example the distributions relative to Run 1453(006) is shown in Fig. 5. Each distribution was then modelled with a power law function $p_0 \cdot x^{p_1}$ where p_1 is the index of the power law and p_0 the normalization factor. These two parameters were derived with a fitting procedure performed in the interval 50–200 p.e., chosen to exclude from the analysis those pixels where the contribution from the background, faint stars or muons could be not negligible and to guarantee the applicability of the χ^2 statistics having all bins of the six distributions more than 20 samplings.

The final parameters were obtained in two steps with an iterative procedure. All distributions were, at first, fitted leaving p_0 and p_1 as free parameters and later all indices were fixed to the same value computed from the p_1 obtained in the first step. This procedure allowed us to avoid the effects of the correlation between p_0 and p_1 , after the normalization for the exposures, in the fitting procedure, without changing the results. Errors in the fitting parameters are relative to 90% confidence level.

The best fit parameters relative to the first step are shown in Table 2 together with the reduced χ^2 , for the six analysed runs. In all cases, the adopted model well reproduces the distributions being all χ^2 within 2σ of the expected values. Indices are also shown in Fig. 6 as function of time: they are all compatible, within errors, with the constant 2.49 ± 0.02 used in the second step of the fitting procedure. The p_1 parameters obtained in the second step are presented in Fig. 7 and in Table 3, together with the values of the reduced χ^2 that state again the goodness of the model. In the same

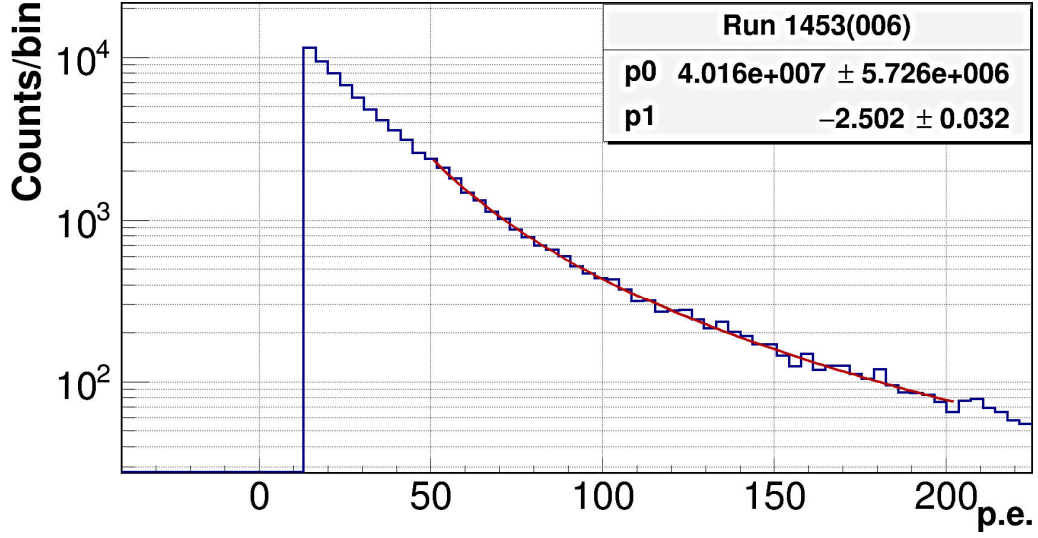


Figure 5. Run 1453(006) p.e. distribution of the images detected in the nine central PDMs. The red curve is the correspondent best fit power law.

table, the rate of the events used for the p.e. distribution and the average NSB fluxes measured by UVscope are also shown.

Table 2. Fitting results for the analysed distributions using a power law model with all parameters free. The reduced χ^2 are relative to 48 dof.

Run ID (Seq.)	p_0 10 ⁴ Counts/bin/s	p_1	χ^2
1453 (006)	3.47±0.49	-2.50±0.03	0.91
1454 (000)	3.33±0.55	-2.52±0.03	1.03
1455 (000)	3.51±0.55	-2.51±0.03	0.90
1455 (005)	3.43±0.59	-2.51±0.04	1.33
1456 (002)	3.33±0.36	-2.48±0.02	0.92
1456 (003)	3.07±0.33	-2.46±0.02	0.94

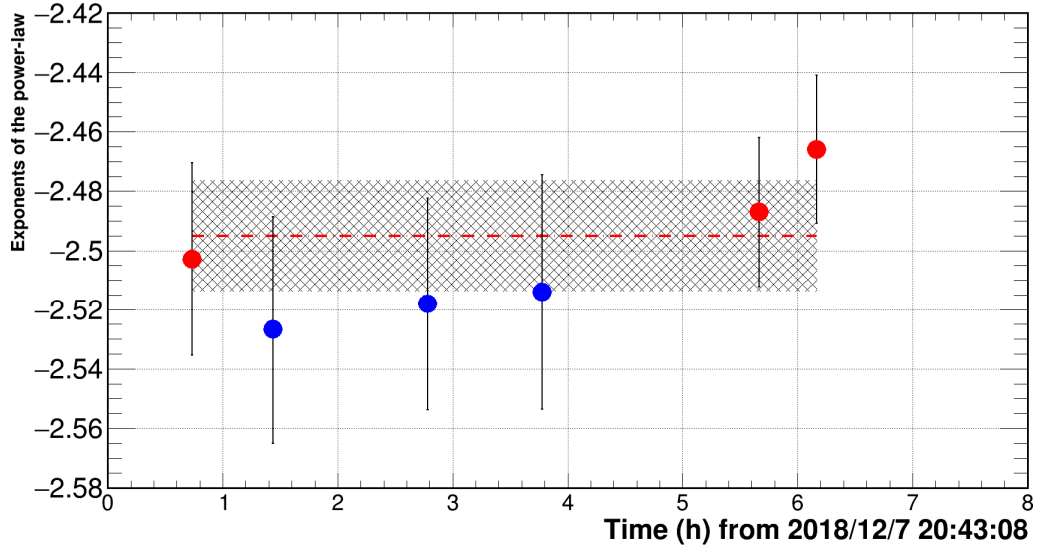


Figure 6. Best fit value of the power law indices vs time obtained from the first step of the fitting procedure leaving both p_0 and p_1 as free parameters. Errors are relative to 90% confidence level.

Table 3. Best fit value of the p_1 obtained from the fit with fixed index (49 dof). The rate of the events used for the p.e. distributions and the UVscope fluxes averaged over the considered intervals are also reported for comparison. Errors in UVscope fluxes are the *RMS* respect to the mean.

Run ID (Seq.)	p_0 10 ⁴ Counts/bin/s	χ^2	Rate (Events/s)	300–650 NSB Flux ph m ⁻² ns ⁻¹ sr ⁻¹
1453 (006)	3.35±0.03	0.89	3.07±0.05	4534±56
1454 (000)	2.94±0.04	1.05	2.83±0.05	5635±84
1455 (000)	3.20±0.04	0.90	3.00±0.05	5141±63
1455 (005)	3.19±0.04	1.32	3.00±0.06	5014±59
1456 (002)	3.45±0.03	0.90	3.11±0.04	4000±52
1456 (003)	3.48±0.03	1.00	3.14±0.04	4014±53

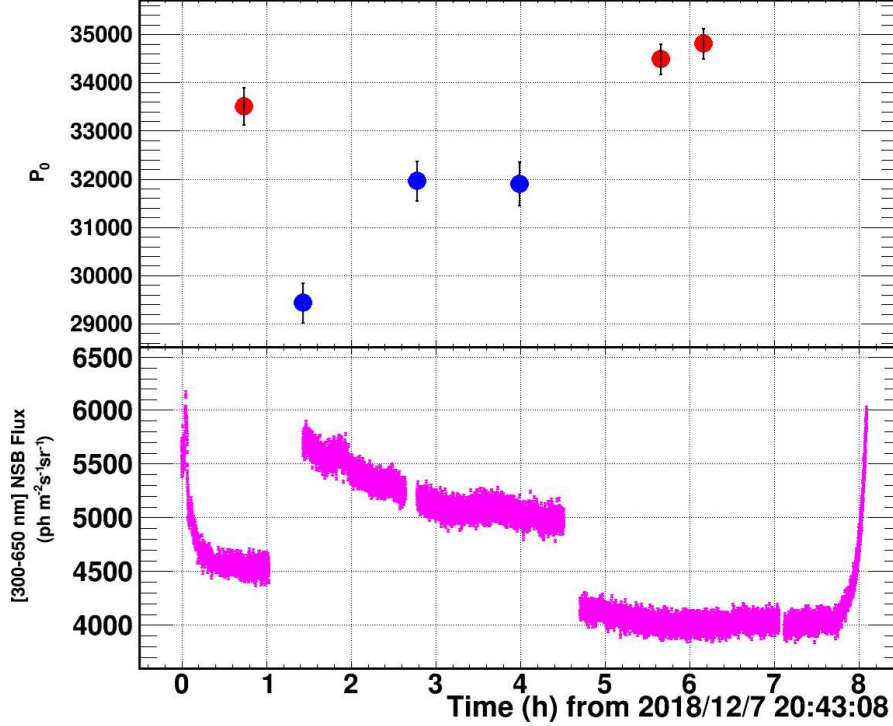


Figure 7. Best fit p_1 values, normalized for the exposures, obtained with fixed indices is shown in the top pane as function of the time: red points are relative to runs not affected by gain reduction, while the blue ones mark intervals with nominal functioning. Errors are relative to 90% confidence level. The contemporary NSB flux measured by UVscope is shown in the bottom panel.

4 Results and Discussion

The p.e. distribution used in our analysis, which depends on the rate of detected events, should not have been correlated to the NSB levels if the camera had operated in nominal regime. However, results presented in Fig. 7 show that the time intervals non affected by current limitation have compatible normalization values (within statistical errors or within the 2% calibration systematic), while significant decreases are detected in the interval with high NSB levels (time $1^h:30'$ to $4^h:30'$ from the observation starting time). The maximum decrease ($\sim 15\%$) is observed in correspondence of the highest level of the diffuse NSB.

A detailed comparison of the results obtained from the signal and from the background analysis is necessary to asses that the current limitation affects both at the same level. To this purpose, we evaluated the percentage gain variations from the nominal values in both data sets:

Signal: in this case, the nominal normalization was obtained averaging the values relative to the runs 1456(002) and 1456(003), when the level of NSB was the lowest. The percentage variations was then computed with respect to this value for all other runs. Results are shown in the top panel of Fig. 8 with black dots.

NSB: in this data set, the evaluation of the NSB statistical variance for each pixel should has been based on the Variance data obtained by the camera electronics [20]. Unfortunately these data were not available in December 2018 due to a technical problem. To overcome such absence, the NSB

variance, hereafter named *PDHVAR*, has been computed as the square of the signal RMS around the pedestal [13]. Note that a check when Variance data were present, as in March 2019, confirmed that the two values are equivalent within a systematic error of 1% [13]. For our analysis, we fitted the *PDHVARs* in the interval relative to each considered Run with a constant and computed the differences (in percentage) with respect to the best fit line of the linear regime (blue dashed line in Fig. 8); obviously for values below 4700 $\text{ph m}^{-2} \text{ns}^{-1} \text{sr}^{-1}$ these differences are compatible with zero. Resulting values are shown in Fig. 8 with triangles.

It is well evident from Fig. 8, that the gain variations detected with the two analyses are compatible within errors. We can then conclude that the phenomenon, induced by the high level of NSB, affects equally the background and the shower signals.

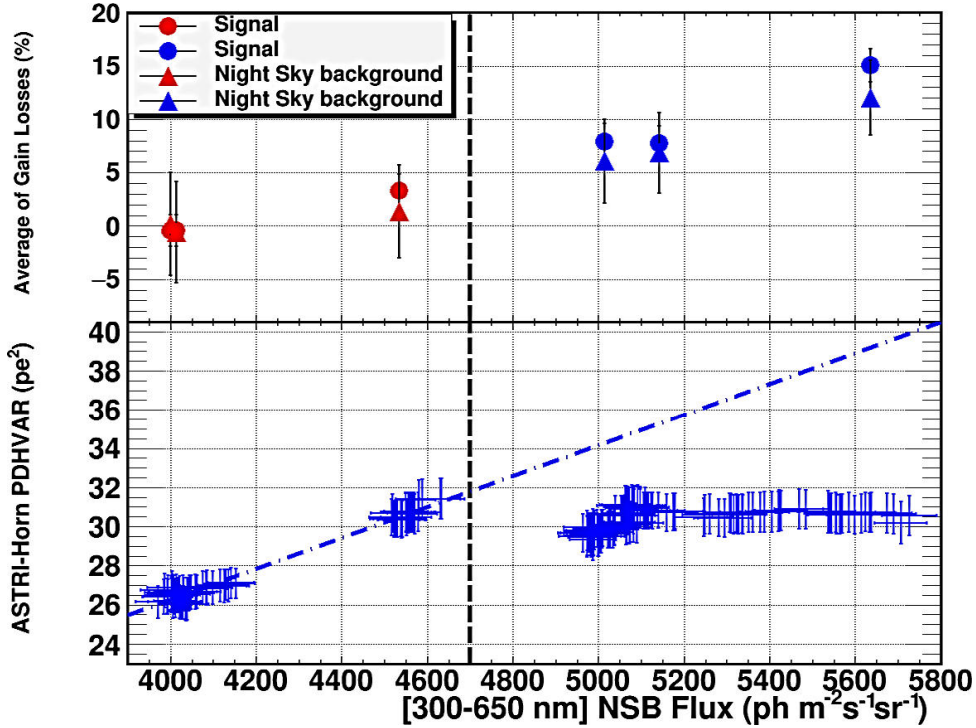


Figure 8. The top panel shows the efficiency losses, in percentage, computed from the *PHDVAR* (dots) and from the fast signals (triangles) as function of the UVscope fluxes. The bottom panel shows the ASTRI-Horn *PHDVARs* vs 300-650 nm NSB fluxes (*PHDVAR* = RMS^2 , see [13]). The blue dash-dotted line indicates the best fit in the nominal working regime. The dashed vertical line indicates the level above which the camera is affected by current limitation.

It follows that, in the analysed data, the gain reduction affects only the observations with the telescope pointing at the Crab Nebula where a high level of NSB is present (see Fig. 3). The gain correction presented in this paper therefore would lead, if applied, to an improvement of the already important result of the Crab detection statistical significance (5.4σ) published in [7] where the number of background events from the OFF-source intervals was corrected only for the different observing time (factor $\alpha=0.88$).

We computed this further correction factor to be applied to OFF-source background events under

simplified assumption. The gain reductions produce an increase of the telescope lower energy threshold and a consequent reduction of the background event rate. To quantify this, we computed the event rates used for the p.e. distributions in each acquisition (see Table 3), and assumed that the same reduction factor could be applied to the total number of background events (233 ± 14) published in [7]. We found a rate reduction between 4% and 10% during ON-source pointings, that converts in an increase of the Crab detection statistical significance of 5.8 and 6.3σ , respectively.

5 Summary and Conclusions

In this paper, we presented results on the gain variation that affected the shower signal detected by ASTRI-Horn as consequence of the increase of the NSB flux, even if the gain calibration of each camera pixel performed periodically with the FOC presented a stable behaviour at level of 2% along all the 2018-2019 observations. The analysis presented in this paper was performed using a set of data collected on December 2018. We found that only data collected during Crab pointings were affected by gain reduction with a maximum of $\sim 15\%$ observed in correspondence of the highest NSB level of $5635 \text{ ph m}^{-2} \text{ ns}^{-1} \text{ sr}^{-1}$ ($1.71 \text{ m}^{-2} \text{ ns}^{-1} \text{ deg}^{-2}$). Off-source data, on the contrary, are relative to a nominal functioning of the camera. Moreover, the levels of gain variation measured with our current analysis is compatible within the errors with those obtained from the background *RMS* as presented in our previous work [13].

The limit in the PDM power system of ASTRI-Horn has been upgraded to reduce this problem. The new power system will be able to supply a constant power up to $\sim 12 \text{ mA}$ that will allow us for a correct observation in dark time (Moon illumination $< 40\%$). Furthermore, this limit has been moved to $\sim 70 \text{ mA}$ for the telescopes of ASTRI Mini-Array to make them able to observe also in grey conditions (Moon illumination between 40% and 70% and Moon minimum angular distance $> 90^\circ$).

The main point that this paper highlighted is the importance of having a contemporary measurements of the level of NSB, not only for a better modelling the background level in shower images, but also as diagnostic tool for the correct functioning of the telescope.

To this purpose, UVSiPM, an upgraded version of UVscope is foreseen for the ASTRI Mini-Array. This will use the same sensors and the same filter as the telescope cameras for simpler correlation between the two instruments. In extreme observing conditions, as with high Moon illumination, the use of this auxiliary instrument would be very useful in supporting the scientific analysis.

Acknowledgments

This work was conducted in the context of the ASTRI Project, supported by the Italian Ministry of Education, University, and Research (MIUR) with funds specifically assigned to the Italian National Institute of Astrophysics (INAF), and by the Italian Ministry of Economic Development (MISE) within the Astronomia Industriale program. This work has gone through internal review by the ASTRI Project Collaboration.

Data Availability Statement: The data analysed during the current study are not publicly available being taken during the commissioning phase of the telescope, but are available from the corresponding author on reasonable request.

Conflicts of Interest: The authors declare that they have no conflicts of interest.

References

- [1] T. Weekes, *Very high energy gamma-ray astronomy - On the threshold*, *Annals of the New York Academy of Sciences* **571** (1989) 372.
- [2] A. Daum, A. Hermann and G.H. et al., *First results on the performance of the HEGRA IACT array*, *Astroparticle Physics* **8** (1997) 1.
- [3] N. Park and VERITAS Collaboration, *Performance of the VERITAS experiment*, in *34th International Cosmic Ray Conference (ICRC2015)*, vol. 34 of *International Cosmic Ray Conference*, p. 771, July, 2015 [[1508.07070](#)].
- [4] J. Aleksić., S. Ansoldi, L. Antonelli and et al., *The major upgrade of the MAGIC telescopes, Part II: A performance study using observations of the Crab Nebula*, *Astroparticle Physics* **72** (2016) 76 [[1409.5594](#)].
- [5] A. Konopelko, *STEREO ARRAY of 30 m imaging atmospheric Čerenkov telescopes: A next-generation detector for ground-based high energy gamma-ray astronomy*, *Astroparticle Physics* **24** (2005) 191 [[astro-ph/0506465](#)].
- [6] H. Anderhub, M. Backes, A. Biland and et al., *FACT – the First Cherenkov Telescope using a G-APD Camera for TeV Gamma-ray Astronomy (HEAD 2010)*, *arXiv e-prints* (2010) arXiv:1010.2397 [[1010.2397](#)].
- [7] S. Lombardi, O. Catalano, S. Scuderi and et al., *First detection of the Crab Nebula at TeV energies with a Cherenkov telescope in a dual-mirror Schwarzschild-Couder configuration: the ASTRI-Horn telescope*, *Astronomy and Astrophysics* **634** (2020) A22 [[1909.12149](#)].
- [8] The CTA Consortium, *Design concepts for the Cherenkov Telescope Array CTA: an advanced facility for ground-based high-energy gamma-ray astronomy*, *Experimental Astronomy* **32** (2011) 193 [[1008.3703](#)].
- [9] L.A. Antonelli and Astri Collaboration, *The ASTRI Mini-Array at Teide Observatory*, in *37th International Cosmic Ray Conference*, p. 897, Mar., 2022, [DOI](#).
- [10] S. Vercellone, C. Bigongiari, A. Burtovoi and et. al., *ASTRI Mini-Array Core Science at the Observatorio del Teide*, *Journal of High Energy Astrophysics* **35** (2022) .
- [11] M. Maccarone, G. Leto, P. Bruno and et al., *The Site of the ASTRI SST-2M Telescope Prototype*, in *International Cosmic Ray Conference*, vol. 33 of *International Cosmic Ray Conference*, p. 2795, Jan., 2013, [DOI](#) [[1307.5139](#)].
- [12] M. Maccarone, G. La Rosa, O. Catalano and et al., *UVscope and its application aboard the ASTRI-Horn telescope*, *Experimental Astronomy* (2021) [[2103.02233](#)].
- [13] A. Compagnino, T. Mineo, M. Maccarone and et al, *Evaluating the night sky background directly from the signal images detected by the ASTRI telescopes*, *Experimental Astronomy* **53** (2022) 1017.
- [14] G. Horn d'Arturo, *The tessellated mirror*, *Journal of the British Astronomical Association* **63** (1953) 71.

- [15] S. Lombardi, L. Antonelli, C. Bigongiari, et al. and for the ASTRI Collaboration, *Performance of the ASTRI Mini-Array at the Observatorio del Teide*, in *37th International Cosmic Ray Conference*, p. 884, Mar., 2022, [DOI](#).
- [16] V. Vassiliev, P. Fegan and P. Brousseau, *Wide field aplanatic two-mirror telescopes for ground-based γ -ray astronomy*, *Astroparticle Physics* **28** (2007) 10 [[astro-ph/0612718](#)].
- [17] O. Catalano, et al. and ASTRI Collaboration, *The ASTRI camera for the Cherenkov Telescope Array*, in *Proceedings of the SPIE*, vol. 10702 (2018), [DOI](#).
- [18] G. Sottile, O. Catalano, G. La Rosa, et al. and for the ASTRI Collaboration, *ASTRI SST-2M camera electronics*, in *Ground-based and Airborne Telescopes VI*, H.J. Hall, R. Gilmozzi and H.K. Marshall, eds., vol. 9906 of *Society of Photo-Optical Instrumentation Engineers (SPIE) Conference Series*, p. 99063D, July, 2016, [DOI](#).
- [19] J. Fleury, S. Callier and C.d. et al., *Petiroc and Citiroc: front-end ASICs for SiPM read-out and ToF applications*, *Journal of Instrumentation* **9** (2014) C01049.
- [20] A. Segreto, O. Catalano, M. Maccarone, et al. and for the ASTRI Collaboration, *Calibration and monitoring of the ASTRI-Horn telescope by using the night-sky background measured by the photon-statistics ("variance") method*, in *36th International Cosmic Ray Conference (ICRC2019)*, vol. 36 of *International Cosmic Ray Conference*, p. 791, July, 2019 [[1909.08750](#)].
- [21] O. Catalano, M. Maccarone and B. Sacco, *Single photon counting approach for imaging atmospheric Cherenkov telescopes*, *Astroparticle Physics* **29** (2008) 104.